Synthesis and Characterization of Hematite Nanowires/Nanorods as Active Photocatalyst for Water Splitting Application

by

Chin Sze Mei

Dissertation submitted in partial fulfillment of
the requirements for the
Bachelor of Engineering (Hons)
(Chemical Engineering)

SEPTEMBER 2012

Universiti Teknologi PETRONAS
Bandar Seri Iskandar
31750 Tronoh
Perak Darul Ridzuan

CERTIFICATION OF APPROVAL

Synthesis and Characterization of Hematite Nanowires/Nanorods as Active Photocatalyst for Water Splitting Application

by

Chin Sze Mei

A project dissertation submitted to the
Chemical Engineering Programme
Universiti Teknologi PETRONAS
in partial fulfilment of the requirement for the
BACHELOR OF ENGINEERING (Hons)
(CHEMICAL ENGINEERING)

Approved by,

_____

(Dr. Suriati bt Sufian)

UNIVERSITI TEKNOLOGI PETRONAS
TRONOH, PERAK
September 2012

CERTIFICATION OF ORIGINALITY

This is to certify that I am responsible for the work submitted in this project, that the original work is my own except as specified in the references and acknowledgements, and that the original work contained herein have not been undertaken or done by unspecified sources or persons.

_____

CHIN SZE MEI

ABSTRACT

Renewable energy and environmental issues are highly emphasized globally in order to replace and reduce the use of fossil fuels in various sectors. Thus, the research on hydrogen gas production has been done since decades ago as an alternative for renewable energy. Photocatalytic water splitting is one of the methods to produce hydrogen gas by using photocatalysts such as hematite. There are various methods to synthesize hematite nanostructures. However, the use of self-combustion method to synthesize hematite is still limited and under investigation. In addition, the effects of stirring period on the characteristics of the hematite nanostructures produced from self-combustion method have yet to be known from the studies. Thus, the objectives of this research are to synthesize and characterize hematite nanowires/nanorods by using self-combustion method based on different stirring period as well as to determine the effects of hematite synthesized on photocatalytic activity to produce hydrogen gas from water. This project highlights on the hydrogen production through photocatalytic activity by using hematite nanowires/nanorods synthesized from self-combustion method based on different stirring period. The morphologies and microstructures of the nanostructures are determined using Field-Emission Scanning Electron Microscope (FESEM), X-Ray Diffractometer (XRD) and Particle Size Analyser (PSA). Besides that, Brunauer-Emmett-Teller (BET) surface area analyser is used to determine the surface area of the hematite samples. The hematite nanocatalyst as-synthesized are proven to be rhombohedral crystalline hematite (α-Fe_2O_3) with diameters ranging from 60-140 nm. The BET surface area of hematite samples increased with increasing stirring period. This caused the amount of hydrogen gas produced from photocatalytic water splitting to increase as well.

ACKNOWLEDGEMENT

First of all, I would like to acknowledge my supervisor, Dr. Suriati for guiding me throughout this project by providing me useful information and extra knowledge on the topic. Besides that, I would like to express my deepest gratitude to Mr. Jeefferie who had guided me during the early stages of the project by providing me extra information and methodology to synthesize the samples. Not to forget a special thanks to Mr. Abdus Salam who helped me a lot in operating the hydrogen detector for the photocatalysis part of the project. Apart from that, I would like to thank the lab technicians at Block 3, Block 4 and Block 5 who had helped me as well as providing me apparatus and chemical consumables during my experiments. Without all these helps, I would not have completed this project within the designated period. Thank you.

TABLE OF CONTENTS

CERTIFICATION . . . . . **ii**

ABSTRACT . . . . . **iv**

ACKNOWLEDGEMENT . . . . . **v**

LIST OF FIGURES . . . . . **viii**

LIST OF TABLES . . . . . **ix**

ABBREVIATIONS AND NOMENCLATURES . . . . **x**

CHAPTER 1: INTRODUCTION **1**

1.1 Background of Study 1
1.2 Problem Statement 2
1.3 Objectives 2
1.4 Scope of Study 3

CHAPTER 2: LITERATURE REVIEW **4**

2.1 Background of Photocatalytic Hydrogen Production . 4
2.2 Water Splitting 5
2.3 Photocatalytic Mechanism 6
2.4 Hematite Photocatalyst 8
2.5 Characterization of Hematite Nanostructures . 8
2.6 Types of Synthesis 10

CHAPTER 3: METHODOLOGY **15**

3.1 Calculations for Reactants Used . . 16
3.2 Synthesis of Hematite Nanocatalyst: Sol-Gel Method 16
3.3 Measurement of Photocatalytic Activity: Detection of Hydrogen Production 19
3.4 Calculations for Quantification of Hydrogen Production 20
3.5 List of Chemicals, Apparatus and Equipment 21
3.6 Gantt Chart and Key Milestone . . 23

CHAPTER 4: RESULTS AND DISCUSSION . . . **26**

4.1 Synthesis of Hematite Nanocatalyst . . 26
4.2 Characterization of Hematite Nanocatalyst . 26
4.2.1 X-Ray Diffraction (XRD) . . 26

4.2.2 Particle Size Distribution (PSD) . 29
4.2.3 Field-Emission Scanning Electron Microscopy (FESEM) . 31
4.2.4 Surface Area of Samples . . 36
4.3 Measurement of Photocatalytic Activity . 37

CHAPTER 5: CONCLUSION AND RECOMMENDATIONS . 39
5.1 Conclusion 39
5.2 Recommendations 39

REFERENCES 40

LIST OF FIGURES

Figure 2.1	Schematic diagram of an electrochemical photocell. (1) n-type TiO_2 electrode; (2) platinum back counter electrode; (3) ionically conducting separator; (4) gas burette; (5) load resistance and (6) voltmeter.	4
Figure 2.2	Photosynthesis by green plants and photocatalytic water splitting as an artificial photosynthesis.	5
Figure 2.3	Principle of water splitting on semiconductor photocatalysts.	6
Figure 2.4	Main processes in photocatalytic water splitting.	7
Figure 2.5	Typical XRD patterns of hematite synthesized.	8
Figure 2.6	Typical FESEM image of hematite nanorods.	9
Figure 2.7	Typical TEM and HRTEM images of hematite nanorods and nanotubes.	9
Figure 3.1	General methodology of project.	15
Figure 3.2	Procedures to prepare α-Fe_2O_3 nanocatalyst using self-combustion method.	17
Figure 3.3	Mixture of iron (III) nitrate and nitric acid during stirring period.	18
Figure 3.4	Homogeneous solution during heating time.	18
Figure 3.5	Combusted sample after being dried overnight in oven.	18
Figure 3.6	Experimental setup during measurement of photocatalytic activity.	19
Figure 4.1	Hematite nanocatalyst obtained from self-combustion method.	26
Figure 4.2	XRD patterns of the hematite nanocatalyst samples after stirring for (a) 1 week, (b) 2 weeks, (c) 3 weeks and (d) 4 weeks respectively.	28
Figure 4.3	Particle size distribution for sample S1.	29

Figure 4.4	Particle size distribution for sample S2.	29
Figure 4.5	Particle size distribution for sample S3.	30
Figure 4.6	Particle size distribution for sample S4.	30
Figure 4.7	FESEM image of S1 hematite nanocatalyst sample.	32
Figure 4.8	Diameters of the as-obtained S1 hematite nanocatalyst sample.	32
Figure 4.9	Distribution of S1 hematite nanocatalyst sample.	33
Figure 4.10	EDX spectrum of S1 hematite nanocatalyst sample.	33
Figure 4.11	FESEM image of S4 hematite nanocatalyst sample.	34
Figure 4.12	Diameters of the as-obtained S4 hematite nanocatalyst sample.	34
Figure 4.13	Distribution of S4 hematite nanocatalyst sample.	35
Figure 4.14	EDX spectrum of S4 hematite nanocatalyst sample.	35
Figure 4.15	SEM images of hematite nanostructures synthesized by Liu et. al.	36

LIST OF TABLES

Table 2.1	Types of synthesis and findings for hematite nanostructures.	10
Table 3.1	List of chemicals, apparatus and equipment used for the project.	21
Table 3.2	Gantt chart used for FYP I.	23
Table 3.3	Gantt chart used for FYP II.	24
Table 3.4	Gantt chart used for experimental works during FYP I and FYP II.	25
Table 4.1	BET surface area of S1, S2, S3 and S4 hematite nanocatalyst samples.	37
Table 4.2	Amount of hydrogen gas produced from S1, S2, S3 and S4 hematite nanocatalyst samples.	38

ABBREVIATIONS AND NOMENCLATURES

BET	Brunauer-Emmett-Teller
CB	Conduciton Band
EDX	Energy-dispersive X-ray
FESEM	Field-Emission Scanning Electron Microscope/Field-Emission Scanning Electron Microscopy
HRTEM	High-Resolution Transmission Electron Microscope
PSA	Particle Size Analyser
PSD	Particle Size Distribution
UV	Ultra-violet
VB	Valence band
XRD	X-Ray Diffractometer/X-Ray Diffraction

CHAPTER 1

INTRODUCTION

1.1 Background of Study

Renewable energy and environmental issues are highly emphasized globally in order to replace and reduce the use of fossil fuels in various sectors. Hydrogen has emerged to be a competitive form of renewable energy because it is clean, safe, and economical and can be used in fuel cells as well. Currently, it is mainly produced by steam reforming of hydrocarbons such as methane in industry through the reactions shown below [1,2,3].

$$\mathbf{CH_4 + H_2O \rightarrow CO + 3\,H_2} \quad \mathbf{(1)}$$

$$\mathbf{CO + H_2O \rightarrow CO_2 + H_2} \quad \mathbf{(2)}$$

However, in this process, fossil fuels are consumed and CO_2 is emitted to the environment which increases the amount of greenhouse gases in the atmosphere. So, due to the environmental issues and concern about depletion of natural resources, production of hydrogen gas from water by using renewable energy sources such as the sun has been discovered and developed. There are several ways to produce hydrogen from solar energy [3]:

i. Electrolysis of water using a solar cell, a hydroelectric power generation, etc.
ii. Reforming of biomass.
iii. Photocatalytic or photoelectrochemical water splitting.

Water splitting has been studied in the research fields of catalysis, electrochemistry, photochemistry, organic and inorganic chemistry since the discovery of Honda-Fujishima effect by using a TiO_2 semiconductor electrode in hydrogen production [4]. Since TiO_2 photocatalyst can only make use of the UV radiation which occupies only 4% of the solar energy [5], many photocatalysts with better properties have been developed in order to replace TiO_2.

From all the photocatalysts discovered and developed, hematite (α-Fe_2O_3) has been synthesized to be one of the candidates developed for photocatalysis in water splitting application. It is the mineral form of iron (III) oxide and is considered as the

most stable iron oxide. It has emerged as one of the promising photocatalysts in water splitting application because of its attractive properties such as small band gap (2.1 eV), high resistivity to corrosion, low cost and abundant [6].

1.2 Problem Statement

Many research works are focusing on synthesis of hematite nanostructures leading to the development of various synthesis methods. Different synthesis methods are being developed and used by researchers to synthesize hematite nanostructures. From these methods, different morphologies of hematite nanostructures are being synthesized. However, synthesis of hematite nanostructures using self-combustion method is still limited and under investigation. In addition, the effects of stirring period on the characteristics of the hematite nanostructures produced from self-combustion method have yet to be known from the studies. Thus, this research proposed to synthesize hematite nanostructures using self-combustion method based on different stirring period and observe their effects on photocatalytic activity to produce hydrogen gas from water.

1.3 Objectives

The main objectives of this project are:

- To synthesize and characterize hematite nanowires or nanorods by using self-combustion method based on different stirring period.
- To determine the effects of hematite synthesized in photocatalytic activity to produce hydrogen gas from water.

1.4 Scope of Study

The scope of study of this project will cover the following aspects:

- Synthesizing hematite nanostructures using self-combustion method based on different stirring period.
- Performing characterization of hematite nanostructures using X-Ray Diffractometer (XRD), Particle Size Analyser (PSA), Field-Emission Scanning Electron Microscope (FESEM) and Brunauer-Emmett-Teller surface area analyser (BET).
- Investigating the effects of hematite synthesized in photocatalytic water splitting by quantifying the hydrogen gas produced.

CHAPTER 2

LITERATURE REVIEW

2.1 Background of Photocatalytic Hydrogen Production

The photoelectrochemical effect in TiO_2 to produce hydrogen from water has been discovered in the late 1960s by Honda and Fujishima [4]. From their study, photocurrent flowed from the platinum electrode to the TiO_2 electrode through the external circuit when the surface of TiO_2 was irradiated with light ($\lambda < 415$ nm). The study revealed that oxygen was generated at TiO_2 electrode through oxidation reaction while hydrogen was produced at the Pt electrode through reduction reaction as shown below [4]:

$$\mathbf{TiO_2 + 2\ hv \rightarrow 2\ e^- + 2\ h^+} \quad \mathbf{(3)}$$

$$\mathbf{H_2O + 2\ h^+ \rightarrow (1/2)\ O_2 + 2\ H^+\ (at\ TiO_2\ electrode)} \quad \mathbf{(4)}$$

$$\mathbf{2\ H^+ + 2\ e^- \rightarrow H_2\ (at\ Pt\ electrode)} \quad \mathbf{(5)}$$

The overall reaction is:

$$\mathbf{H_2O + 2\ hv \rightarrow (1/2)\ O_2 + H_2} \quad \mathbf{(6)}$$

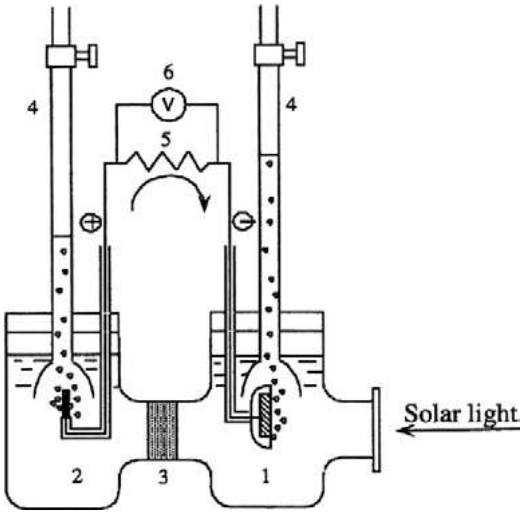

Figure 2.1: Schematic diagram of an electrochemical photocell. (1) n-type TiO_2 electrode; (2) platinum back counter electrode; (3) ionically conducting separator; (4) gas burette; (5) load resistance and (6) voltmeter. [4]

Since then, many studies are done on water splitting by using semiconductor photoelectrodes and photocatalysts because of the success of generation of clean energy from water and solar energy. Meanwhile, a lot of research works are also being done to find other alternatives to replace TiO_2 and enhance the reaction in hydrogen production. It is because TiO_2 can only make use of the UV radiation which occupies only 4% of the solar energy [5] due to its wide band gap energy of around 3.2 eV [6].

2.2 Water Splitting

Water splitting is an uphill reaction which utilizes sunlight to break down water into hydrogen and oxygen. The photon energy from the sunlight is converted to chemical energy with a large positive change in Gibbs free energy (ΔG^o = +237.2 kJ/mol) [3]. Water splitting is also known as artificial photosynthesis because of the uphill reactions as shown in the figure below.

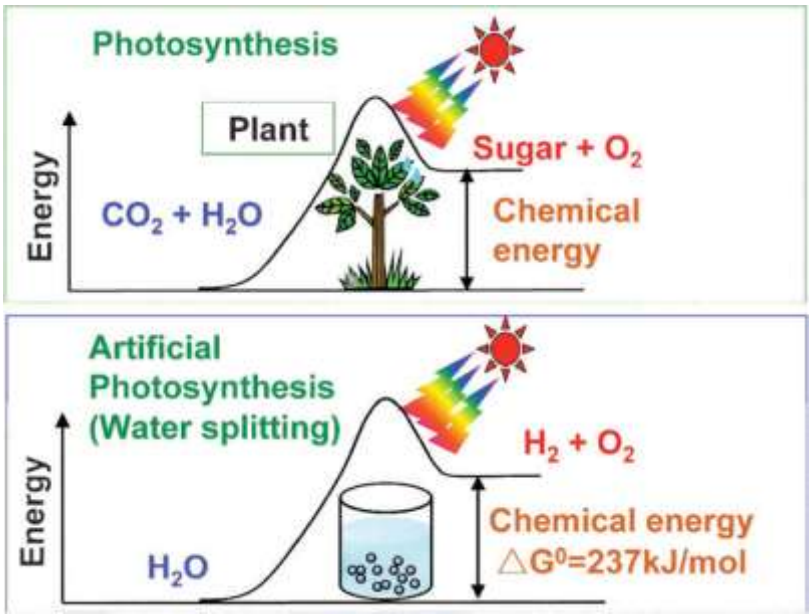

Figure 2.2: Photosynthesis by green plants and photocatalytic water splitting as an artificial photosynthesis. [3]

There are various ways being applied in water splitting, such as by using photoelectrochemical [5,7,8] and photocatalysis [9,10,11].

2.3 Photocatalytic Mechanism

Photocatalytic reaction involves three main processes in order to complete the reaction [2,3]. The first step is absorption of photons to form electron-hole pairs. Water splitting normally occurs on heterogeneous photocatalysts with semiconductor properties. Semiconductors have a band structure in which the conduction band (CB) is separated from the valence band (VB) by a suitable band gap [2,12] as shown in the figure below.

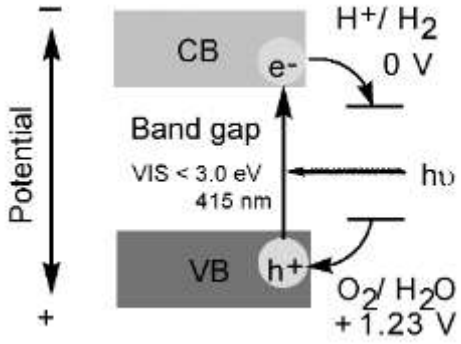

Figure 2.3: Principle of water splitting on semiconductor photocatalysts. [2]

The solar energy has to be larger than the band gap energy, E_g in order for the electrons and holes to be generated in the conduction and valence bands respectively. The photogenerated electrons and holes will cause redox reactions and hydrogen and oxygen will be produced from the water molecules eventually. The relationship between energy and wavelength is represented by the following equations:

$$\boldsymbol{E = hv} \quad \textbf{(7)}$$

where E = energy

h = Planck's constant, 6.63×10^{-34} m^2 kg/s

v = frequency of light

Velocity of light is defined as following:

$$\boldsymbol{c = v\lambda} \quad \textbf{(8)}$$

where c = speed of light, 3×10^8 m/s

λ = wavelength

By substituting equation (8) into (7), the relationship between energy and wavelength of light is shown as below:

$$\boldsymbol{E = h\frac{c}{\lambda}} \qquad \textbf{(9)}$$

This shows that the energy is inversely proportional to the wavelength of light.

The second step in the photocatalytic reaction is the charge separation and migration of photogenerated carriers to the surface of reaction sites. The final step is the surface chemical reactions which complete the overall photocatalytic reaction to produce hydrogen.

Apart from having a suitable band structure, other requirements are needed in order to facilitate the photocatalytic reaction. The crystal structure, crystallinity and particle size will affect the reaction. The better the crystallinity of the particles, the smaller the amount of defects which serve as the recombination sites for the photogenerated electrons and holes. A smaller particle will reduce the distance between photogenerated electrons and holes with the reaction sites thus results in lower recombination probability. Besides that, the number and quality of the active sites for redox reactions are also important for the reaction to happen. A high surface area at the active sites is required in order for the reactions to take place effectively to prevent recombination of photogenerated electrons and holes.

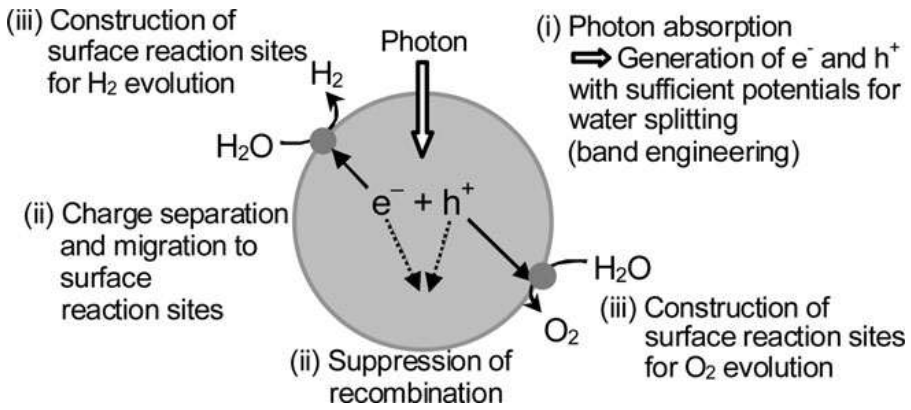

Figure 2.4: Main processes in photocatalytic water splitting. [3]

2.4 Hematite Photocatalyst

Hematite has emerged to be one of the candidate materials for hydrogen production due to its smaller band gap of around 2.1 eV [6,7]. Besides that, it is the most stable iron oxide and has attractive properties such as low cost, abundance and non-toxicity which make it suitable for water splitting applications [7]. It is also widely used in magnetism, lithium ion battery and gas sensors [13]. Hematite nanostructures can be in the form of zero-dimensional (0-D) such as nanoparticles and one-dimensional (1-D) which includes nanowires/nanorods, nanobelts and nanotubes.

2.5 Characterization of Hematite Nanostructures

From the studies done, characterization of hematite nanostructures are normally done by using X-Ray Diffractometer (XRD), Field-Emission Scanning Electron Microscope (FESEM) and High-Resolution Transmission Electron Microscope (HRTEM). XRD can be used to determine the structure of the hematite nanostructures produced. From the figure below, it shows the XRD patterns of hematite nanorods prepared by using surfactant-assisted method [14]. It can be seen that the XRD patterns conform to rhombohedral structure of α-Fe_2O_3 (a = 5.038 Å, c = 13.772 Å, JCPDS Card No. 33-0664) [14].

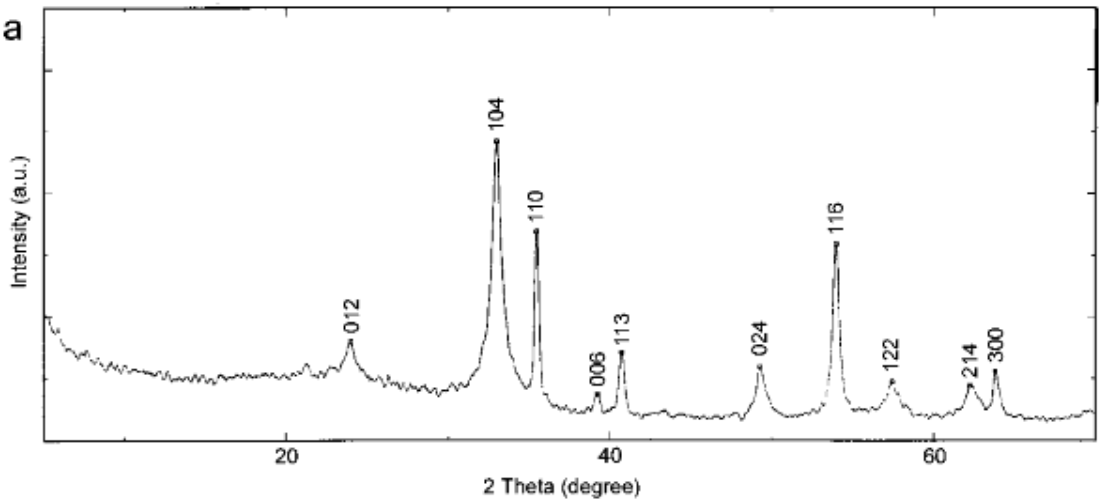

Figure 2.5: Typical XRD patterns of hematite synthesized. [14]

FESEM and HRTEM are used to determine the morphology of the hematite nanostructures produced. The FESEM image as shown below is the hematite nanorods synthesized by using template-free hydrothermal method followed by calcination of intermediate product (α-FeOOH nanorods) [15]. Figure 2.7 shows the TEM and HRTEM images of hematite nanorods and nanotubes synthesized by using surfactant-assisted method [14]. The HRTEM images of the nanorods and selected area electron diffraction (SAED) indicate that they are monocrystalline [14], as shown in Figure 2.7(b).

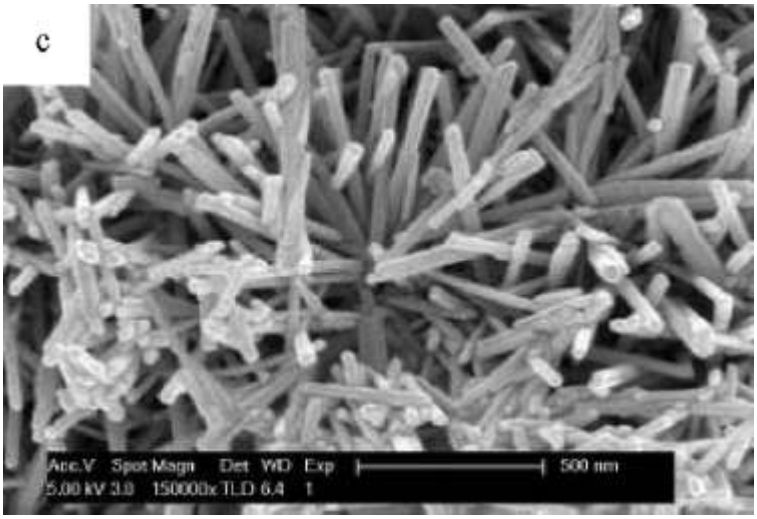

Figure 2.6: Typical FESEM image of hematite nanorods. [15]

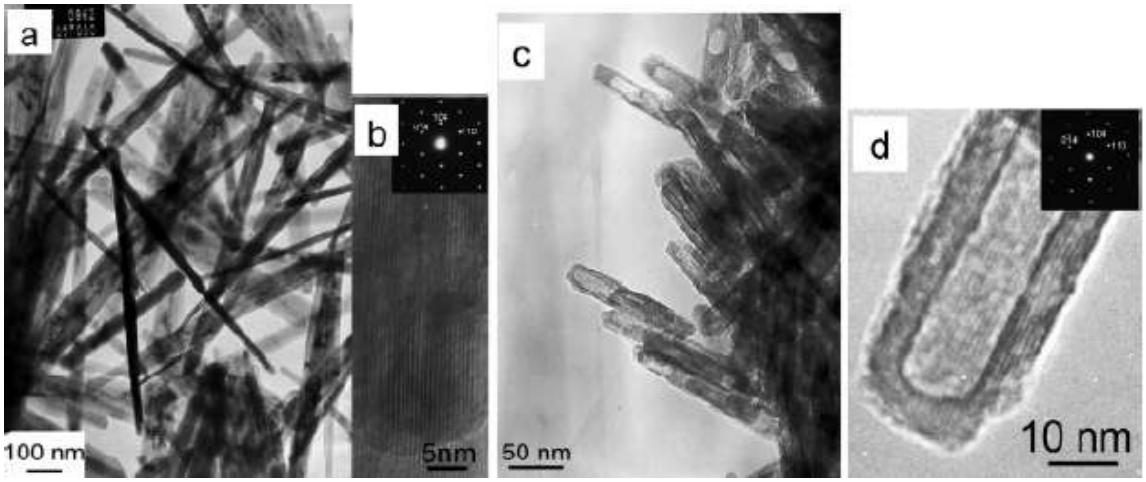

Figure 2.7: Typical TEM and HRTEM images of hematite nanorods and nanotubes. [14]

2.6 Types of Synthesis

Up to date, there are various methods being used to synthesize 1-D hematite nanostructures, namely thermal oxidation of iron [7,13,16], hydrothermal synthesis [9], improved synthetic strategy [13], surfactant assisted synthesis [14], template-free hydrothermal method [15] and also sol-gel method [17]. The findings from these methods are shown in the following table.

Table 2.1: Types of synthesis and findings for hematite nanostructures.

Author / Year	Method	Materials	Operating Parameters	Findings / Remarks
Wang et al. (2005)	Oxidation of pure iron	Annealed pure iron (≥99.96 wt%)	• T = 550°C-600°C • Reaction time = 24 hours • Gas flow = oxidizing gas mixture ($CO_2/N_2/SO_2$, 19.3:80.56:0.14) and H_2O	• Single crystal and bicrystal nanowires are formed • Most of the bicrystalline nanowires are nanotwins with ellipsoidal heads • Nanowires with smaller diameters (≤50nm) tend to form bicrystal structure • Nanowires with larger diameters (≥50nm) tend to have single-crystal structure
Hiralal et al. (2011)	Thermal oxidation in air	Sputter deposited iron films	• T = 255°C • Reaction time = 24 hours	Nanostructured hematite thin films with a higher surface area than typically obtained by directly sputtering hematite were obtained.

Vincent et al. (2012)	Thermal oxidation of iron foils	250 μm thick iron foils (99.9% purity)	• T = 600^{o}C • Reaction time = 8-10 hours • Oxygen to argon gas flow ratio = 1:1	• Hematite nanorods • Thinnest, most vertically oriented and highest aspect ratio nanorod structure
			• T = 700^{o}C • Reaction time = 8-10 hours • Oxygen to argon gas flow ratio = 1:1	• Hematite nanorods • Less uniform array than 600^{o}C sample • Belt-like nanorod shape
			• T = 800^{o}C • Reaction time = 8-10 hours • Oxygen to argon gas flow ratio = 1:1	• Hematite nanorods • Less uniform array than 700^{o}C sample • Wider belt-like nanorod shape
			• T = 700^{o}C • Reaction time = 8-10 hours • Oxygen to argon gas flow ratio = 1:4	• Hematite shows nanocoral morphology
			• T = 400^{o}C-450^{o}C • Reaction time = 24 hours • Air-like environment	• Hematite shows nanoleaf morphology

Liu et al. (2011)	Hydrothermal synthesis	Mixture of $FeCl_3 6.H_2O$ and $(NH_4)_2HPO_4$	• T = 220°C • Reaction time = varied from 3 to 48 hours	• Hematite nanospindles, nanotubes and nanotires are produced respectively with increasing reaction time • The nanospindle and nanotube products were composed by pure hematite • The nanotires consisted of the mixture of hematite and a small amount of complex compound
Wu et al. (2006)	Improved synthetic strategy	FeOOH nanostructures as precursors	• T = 520°C • Reaction time = 8 hours • Precursors: FeOOH nanostructures prepared without inorganic salts	Hematite submicrometer particles with diameter range of 300-500 nm
			• T = 520°C • Reaction time = 8 hours • Precursors: FeOOH nanostructures prepared with NH_4Cl	• Hematite nanorods with porosity and diameter range of 60-90 nm • Regular pores distributed along the hematite nanorods
			• T = 520°C • Reaction time = 8 hours	Mostly solid hematite nanorods with diameters of < 15 nm

			• Precursors: FeOOH nanostructures prepared with KCl	
			• T = 520^{o}C • Reaction time = 8 hours • Precursors: FeOOH nanostructures prepared with Na_2SO_4	Hematite nanorods with porosity and diameter range of 5-19 nm
Zeng et al. (2007)	Template-free hydrothermal method and calcination of intermediate product (α-FeOOH nanorods)	α-FeOOH nanorods prepared by $FeSO_4 \cdot 7H_2O$ and different amount of Na_2SO_3	• T = 500^{o}C • Reaction time = 2 hours • α-FeOOH nanorods prepared with 0.025 mol/L of Na_2SO_3	• A series of hematite nanorods with gradient in aspect ratios were obtained. • As the size of samples increased, the band gaps and discharge capacity of the samples decreased.
Liu et al. (2006)	Surfactant-assisted synthesis	• Carbamide • Aqueous butanol solution	• T = 150^{o}C • Reaction time = 12-15 hours • Surfactant = Polyisobutylene bissuccinimide (L113B)	Hematite nanorods with diameters of 30-50 nm and lengths of 500-1100 nm are obtained.

			• T = 150^{o}C • Reaction time = 12-15 hours • Surfactant = Span80	Hematite nanotubes with diameters of 18-29 nm, wall thicknesses of 3-7 nm, and lengths of 110-360 nm are obtained.
Kim et al. (2001)	Sol-gel method	• Iron powder (99.999% purity) • Nitric acid (98% purity)	• T = 100^{o}C, 140^{o}C, 180^{o}C, 220^{o}C, 350^{o}C • Reaction time = 4 hours • Span80 as surfactant	Single crystal phase structures are obtained except a little bit of the crystal phase of Fe appeared for the samples calcined at 100^{o}C, 140^{o}C and 180^{o}C.

In this paper, the focus will be on the synthesis of hematite nanowires/nanorods by using self-combustion method and determine the effect of different parameters on the characteristics of the nanostructures. The morphologies and microstructures of the synthesized hematite nanostructures will be determined by using FESEM while the crystallinity of the hematite will be characterized by using XRD. Besides that, BET and PSA will be used to determine the surface area and particle size of the hematite respectively. The hematite photocatalyst will be used for water splitting under visible-light irradiation and the amount of hydrogen produced will be quantified through conventional method.

CHAPTER 3

METHODOLOGY

The general methodology of the project is shown in the following diagram.

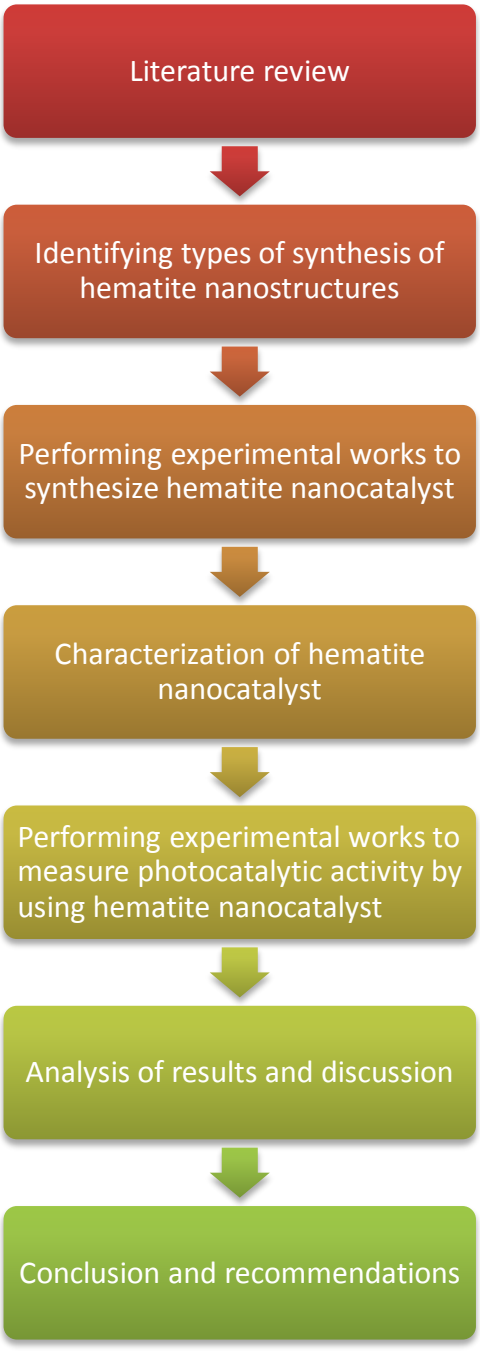

Figure 3.1: General methodology of project.

3.1 Calculations for Reactants Used In Synthesis of Hematite Nanocatalyst

The amount of iron (III) nitrate, $Fe(NO_3)_3.9H_2O$ and nitric acid, HNO_3 used are calculated as shown below:

Estimated amount of hematite that will be produced = 40 g

The reaction equation to form hematite, α-Fe_2O_3 is

$$\mathbf{Fe(NO_3)_3.9H_2O \xrightarrow{HNO_3} \alpha\text{-}Fe_2O_3}$$

Molecular weight of $Fe(NO_3)_3$ = 55.85 + (14.01 × 3) + (16 × 9)

= **241.88 g/mol**

Molecular weight of $Fe(NO_3)_3.9H_2O$ = 55.85 + (14.01 × 3) + (16 × 9) + (18.02 × 9)

= **404.06 g/mol**

Amount of iron (III) nitrate, $Fe(NO_3)_3.9H_2O$ used = (404.06/241.88) × 40 g

= **66.82 g**

Amount of nitric acid, HNO_3 used = 66.82 g × 5 mL

= **334.1 mL**

3.2 Synthesis of Hematite Nanocatalyst: Self-Combustion Method

1. 66.82g of iron (III) nitrate, $Fe(NO_3)_3.9H_2O$ was dissolved in 334.1 mL of 65% nitric acid, HNO_3.
2. The mixture was stirred vigorously on a hot plate at 28^oC by using a magnetic stirrer for 1 week to obtain a homogeneous solution.
3. The homogeneous solution was heated gradually until it combusted at temperature of 110^oC.
4. The gelatine was dried in an oven at 110^oC for overnight.
5. The dried sample was crushed by using mortar and pestle and annealed at 700^oC in a furnace for three hours to get hematite nanocatalyst.

6. Steps 1 to 5 were repeated by changing the stirring period of the mixture to 2 weeks, 3 weeks and 4 weeks respectively. The samples were labelled as S1, S2, S3 and S4 according to their stirring period.
7. The hematite nanocatalyst samples obtained were sent for characterization by using XRD, PSA, FESEM and BET.

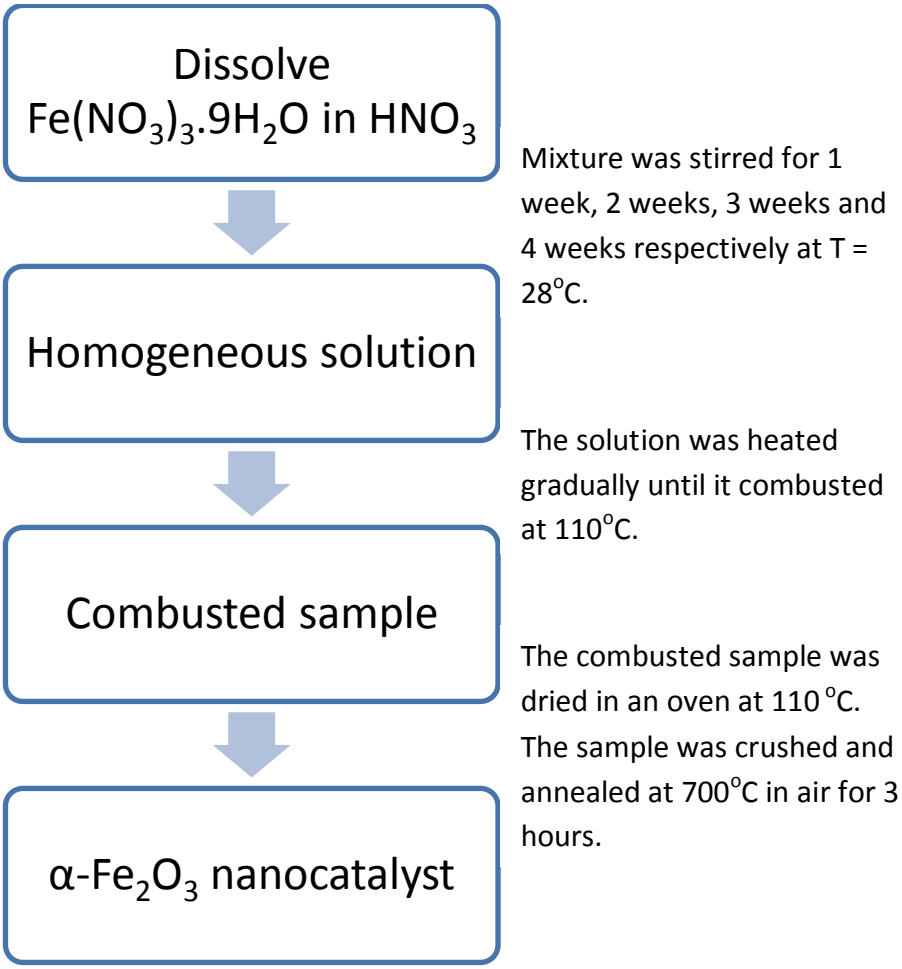

Figure 3.2: Procedures to prepare α-Fe_2O_3 nanocatalyst using self-combustion method.

Figure 3.3: Mixture of iron (III) nitrate and nitric acid during stirring period.

Figure 3.4: Homogeneous solution during heating time.

Figure 3.5: Combusted sample after being dried overnight in oven.

3.3 Measurement of Photocatalytic Activity: Quantification of Hydrogen Production

1. 1g of S1 hematite nanocatalyst sample was mixed in 100 mL of distilled water in a conical flask with side arm.
2. A magnetic stirrer was placed inside the mixture solution and the conical flask tightly was covered using a stopper.
3. The side arm was connected with a small tube and it was immersed into another small conical flask with water.
4. The conical flask containing the mixture solution was placed on top of a hot plate with stirrer. A visible light lamp was installed beside the conical flask.
5. The visible light and the hot plate were switched on. The stirring rate and temperature were set at 300 rpm and 50^{o}C respectively.
6. The experimental setup was covered using a box in order to perform the experiment in a black box condition.
7. The amount of bubbles released from the small tube immersed in small conical flask was recorded for 15 minutes.
8. After 15 minutes of experiment, the light and hot plate were switched off. The amount of hydrogen produced from the solution was calculated.
9. Steps 1 to 8 were repeated with S2, S3 and S4 hematite nanocatalyst samples.

Figure 3.6: Experimental setup during measurement of photocatalytic activity.

3.4 Calculations for Quantification of Hydrogen Production

The rate of hydrogen gas produced from each sample during the photocatalytic activity was calculated using the steps as shown below.

Volume of 1 bubble, $V = (4/3)\pi r^3$

where r = radius of 1 bubble, m

PV = nRT

where P = pressure = 101325 Pa
V = volume of 1 bubble, m^3
n = no. of moles of hydrogen, mol
R = gas constant = 8.314 m^3.Pa/K.mol
T = temperature = 298 K

No. of moles of hydrogen, n = PV/RT
= **A mol**

Mass of hydrogen gas for 1 bubble = A × MW
= **B g**

where MW = molecular weight of hydrogen gas = 2.02 g/mol

No. of bubbles released from the small conical flask = **C**

Mass of hydrogen gas produced = C × B
= **D g**

For 15 minutes of experiment, the rate of hydrogen gas produced = D g/15 min
= E g/min / 60
= **F g/s**

3.5 List of Chemicals, Apparatus and Equipment

The chemicals, apparatus and equipment used for this project are tabulated and described in the following table.

Table 3.1: List of chemicals, apparatus and equipment used for the project.

No.	Chemicals/Apparatus/Equipment	Description
1	Iron (III) nitrate, $Fe(NO_3)_3.9H_2O$	Reactant used to synthesize hematite.
2	65% Nitric acid, HNO_3	Reactant used to synthesize hematite.
3	Electric weighing scale	To weigh the reactants and hematite photocatalyst.
4	Measuring cylinder	To measure the amount of reactant used.
5	Magnetic stirrer	To stir the mixture of iron (III) nitrate and nitric acid. To stir the mixture solution of hematite nanocatalyst and distilled water.
6	Hot plate with stirrer	To stir and heat the solution during reaction.
7	Beakers	To hold the mixture solution during reaction.
8	Thermometer	To record the temperature of the solution during heating.
9	Mortar and pestle	To crush the dried sample.
10	Crucible	To hold the sample during annealing.
11	Watch glass	To hold the hematite sample for further characterization.
12	Conical flask with side arm	To hold mixture solution of hematite photocatalyst and water.
13	Small tube	To connect the side arm of conical flask to allow gas flow during photocatalysis.
14	Visible light lamp	To supply visible light for irradiation during photocatalytic acitivity.
15	X-Ray Diffractometer (XRD)	To study the crystallography of the

		hematite nanocatalyst samples.
16	Field-Emission Scanning Electron Microscope (FESEM)	To study the surface morphology of the hematite nanocatalyst samples.
17	Particle Size Analyser (PSA)	To study the particle size distribution of the hematite nanocatalyst samples.
18	Brunauer-Emmett-Teller Surface Area Analyser (BET)	To find the surface area of the hematite nanocatalyst samples.

3.5 Gantt Chart and Key Milestone

The Gantt charts used for FYP I, FYP II and experimental works in this project are shown below.

Table 3.2: Gantt chart used for FYP I.

No.	Activities	Week														
		1	2	3	4	5	6	7	Mid-Semester Break	8	9	10	11	12	13	14
1	Selection of project topic															
2	Preliminary research work															
3	Submission of extended proposal															
4	Proposal defence															
5	Research work continues															
6	Submission of interim draft report															
7	Experimental work begins															
8	Submission of interim report															

Table 3.3: Gantt chart used for FYP II.

No.	Activities	Week														
		1	2	3	4	5	6	7		8	9	10	11	12	13	14	15
1	Experimental works continue																
2	Submission of progress report																
3	Experimental works continue																
4	Submission of draft report																
5	Submission of dissertation (soft bound)																
6	Submission of technical paper																
7	Oral presentation																
8	Submission of project dissertation (hard bound)																

Table 3.4: Gantt chart used for experimental works during FYP I and FYP II.

No.	Experimental Activities	Week													
		FYP I			FYP II										
		15	Exam Week	Sem Break	1	2	3	4	5	6	7	8	9	10	11
1	**Synthesis of hematite nanocatalyst**														
	S4														
	S3														
	S2														
	S1														
2	**Characterization of hematite nanocatalyst**														
3	**Photocatalytic activity**														
	S1														
	S2														
	S3														
	S4														

Where S1 = sample with 1 week stirring period S2 = sample with 2 weeks stirring period

S3 = sample with 3 weeks stirring period S4 = sample with 4 weeks stirring period

CHAPTER 4

RESULTS AND DISCUSSION

4.1 Synthesis of Hematite Nanocatalyst

The four hematite nanocatalyst samples obtained after crushing and annealing appeared in reddish-brown colour as shown in Figure 4.1 below. The reddish-brown colour is the typical colour of α-Fe_2O_3. The samples were sent for characterization by using XRD, PSA, FESEM and BET in which the results will be described in the following sections.

Figure 4.1: Hematite nanocatalyst obtained from self-combustion method.

4.2 Characterization of Hematite Nanocatalyst

4.2.1 X-Ray Diffraction (XRD)

Four of the hematite nanocatalyst samples synthesized have been sent for XRD to study the crystallography of the samples. The XRD patterns were taken using a Bruker-AXS D8 Advance diffractometer with Cu-Kα radiation (λ = 1.5406 Å) operating at 60kV and 80mA. A scan range of 20^o-80^o (2θ) was used. Figure 4.1 below shows the XRD patterns of the hematite nanocatalyst samples after stirring for (a) 1 week, (b) 2 weeks, (c) 3 weeks and (d) 4 weeks respectively.

The peaks shown in the figure matched the standard hematite sample (JCPDS Card No. 33-0664, a = b = 5.0353 Å and c = 13.7495 Å) [13,14,15,20]. The samples showed strong peaks at [012], [104], [110], [024], [116], [214] and [300] which prove that the hematite samples obtained are rhombohedral crystalline hematite (α-Fe_2O_3). The major

XRD peaks for all the samples were obtained at $2\theta \approx 33.15^{o}$ while the second major peaks were observed at $2\theta \approx 35.7^{o}$.

The diameters of the samples are determined by using Scherrer equation as shown below.

$$\boldsymbol{D = \frac{k\lambda}{B\cos\theta}} \quad \textbf{(10)}$$

Where k = constant dependent on crystallite shape

λ = X-ray wavelength

B = FWHM (full width at half maximum)

θ = Bragg angle

The diameter of sample S1 is found to be 470.91 nm and the diameter increases to 471 nm for sample S4. It can be seen that the particle size increased from S1 to S4 with increasing stirring period.

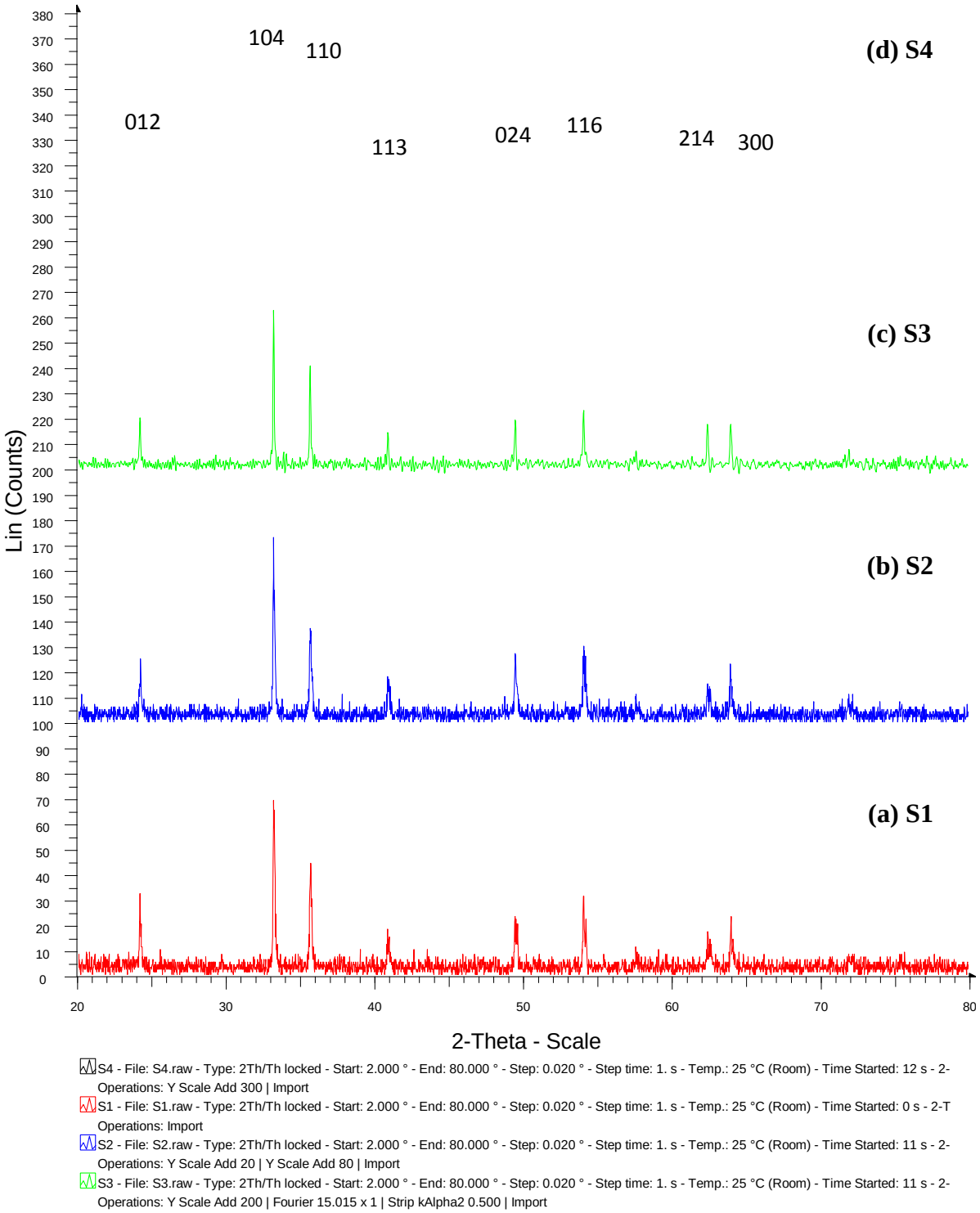

Figure 4.2: XRD patterns of the hematite nanocatalyst samples after stirring for (a) 1 week, (b) 2 weeks, (c) 3 weeks and (d) 4 weeks respectively.

4.2.2 Particle Size Distribution (PSD)

The particle size distribution of the hematite nanocatalyst samples were analysed by using particle size analyser (PSA) by Malvern Instruments. Figures 4.2, 4.3, 4.4 and 4.5 below show the particles size distribution of samples S1, S2, S3 and S4 respectively.

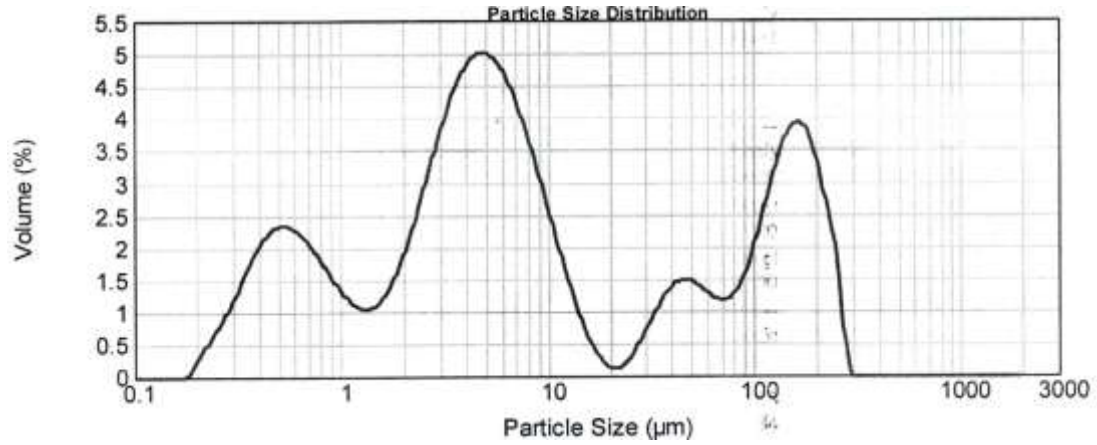

Figure 4.3: Particle size distribution for sample S1.

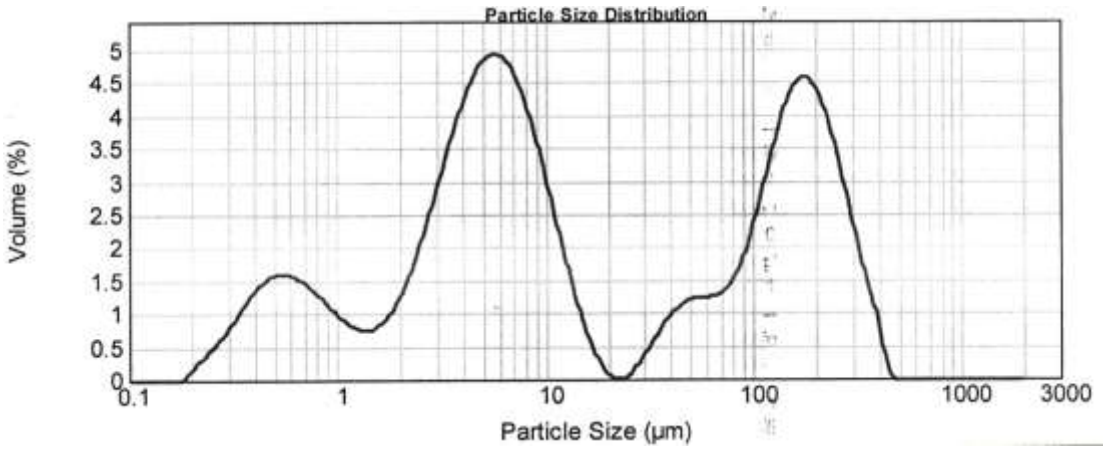

Figure 4.4: Particle size distribution for sample S2.

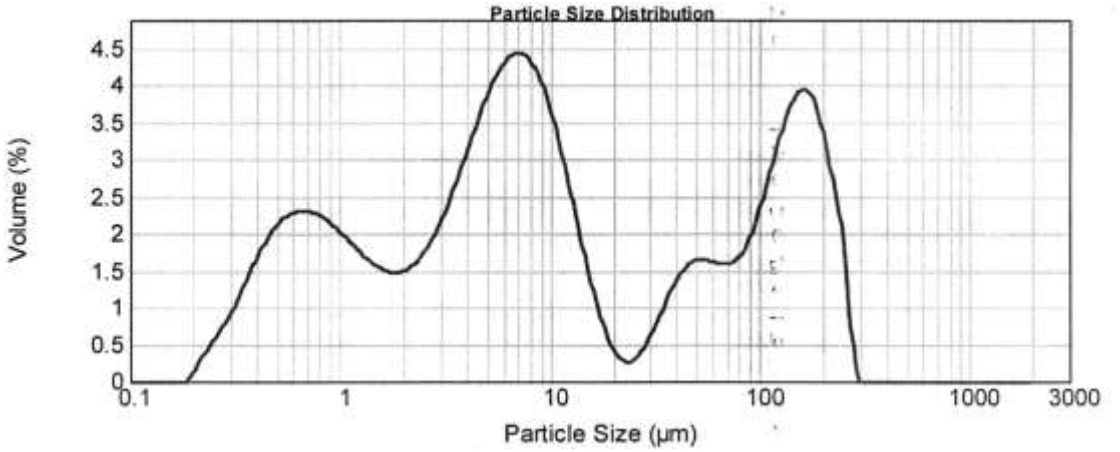

Figure 4.5: Particle size distribution for sample S3.

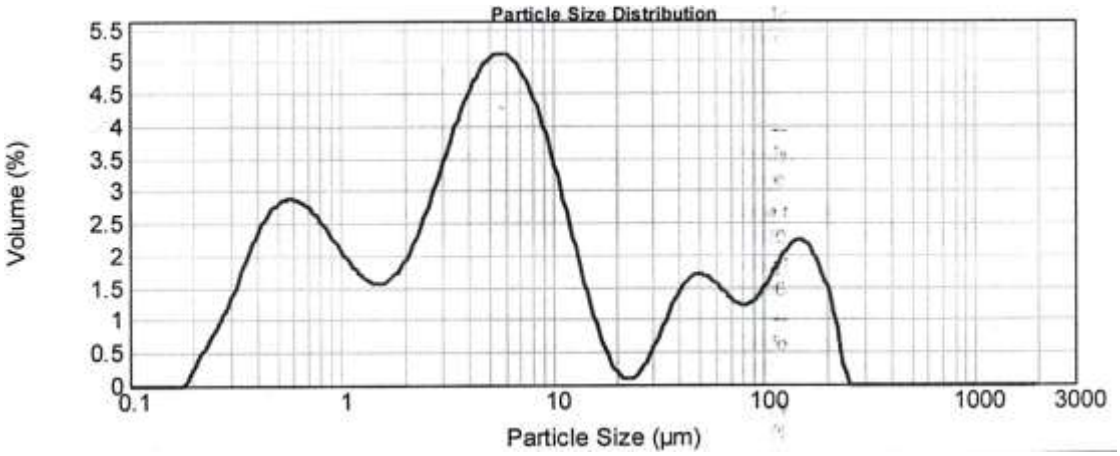

Figure 4.6: Particle size distribution for sample S4.

From the particle size distribution graphs of the samples, it can be seen that most of the particles in samples S1, S2 and S3 are distributed in the size of 4.7 µm and 170 µm. Meanwhile, most of the particles in sample S4 are distributed in the size of 0.59 µm and 5.5 µm. The particle sizes of the hematite nanocatalyst samples determined by PSA are larger than the particle sizes obtained from XRD. This is because PSA can only detect the size of the particles that agglomerate together into big particles, which results in larger particles size distribution of the hematite nanocatalyst samples.

4.2.3 Field-Emission Scanning Electron Microscopy (FESEM)

The S1 and S4 hematite nanocatalyst samples were sent for FESEM to depict the surface morphology of the samples. The model used was Variable Pressure Field-Emission Scanning Electron Microscope (VPFESEM, Zeiss Supra55 VP). Figure 4.7 shows the FESEM image of S1 hematite nanocatalyst sample that has been stirred for 1 week. From the image, it is clearly shown that the hematite nanocatalyst appeared in spherical shape. The diameters of the as-grown hematite nanocatalyst are distributed in the range of 60-120 nm. The EDX spectrum of S1 hematite nanocatalyst sample is shown in Figure 4.10. The sample showed the presence of Fe, O and a small amount of C in weight percentage of 52.03%, 37.83% and 10.13% respectively. This has proven that the as-obtained sample is α-Fe_2O_3.

On the other hand, Figure 4.10 shows the FESEM image of S4 hematite nanocatalyst sample which has been stirred for 4 weeks. The hematite nanocatalyst occurred in spherical shape as well. The diameters of the hematite nanocatalyst are distributed in the range of 90-140 nm, which are slightly larger than S1 hematite nanocatalyst. The EDX spectrum of S4 hematite nanocatalyst sample in Figure 4.14 shows that Fe, O and C are present in 59.70%, 34.42% and 5.88% respectively. The sample is proven to be α-Fe_2O_3.

The FESEM images of S1 and S4 samples are being compared with SEM images of hematite nanoparticles produced by other researchers. It is found that the diameters of the hematite nanostructures synthesized by Liu et. al. (2011) fall within the range of 60-150 nm, which is almost the same as the diameters of S1 and S4 samples [20]. For the increasing time of reaction, the diameters of the hematite nanostructures increase until 200 nm [20]. The SEM images of the hematite nanostructures by Liu et. al. (2011) are shown in Figure 4.15.

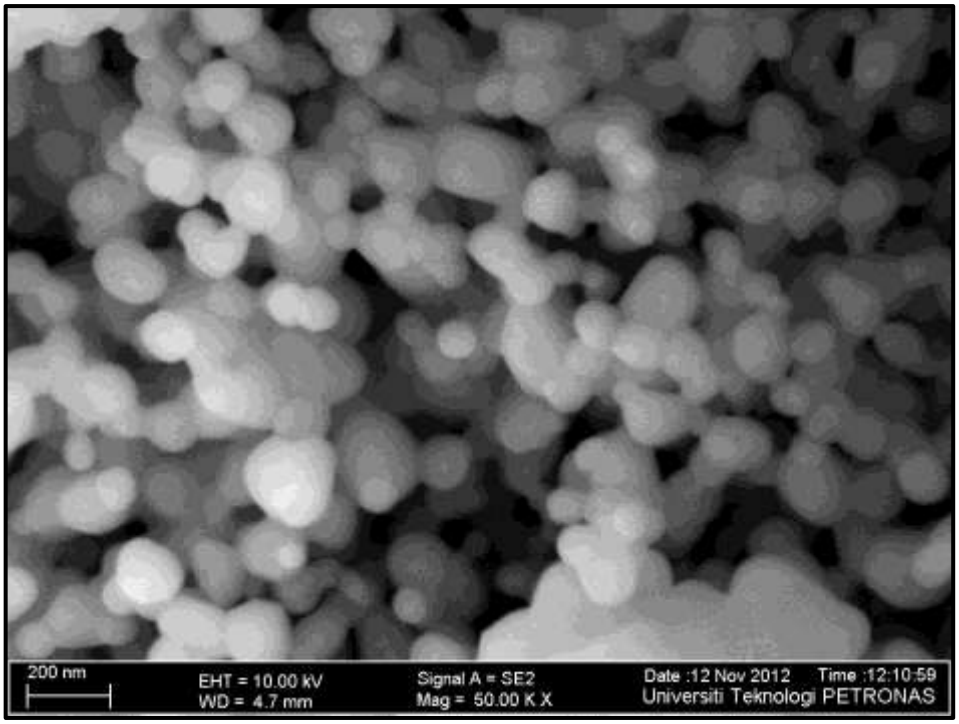

Figure 4.7: FESEM image of S1 hematite nanocatalyst sample.

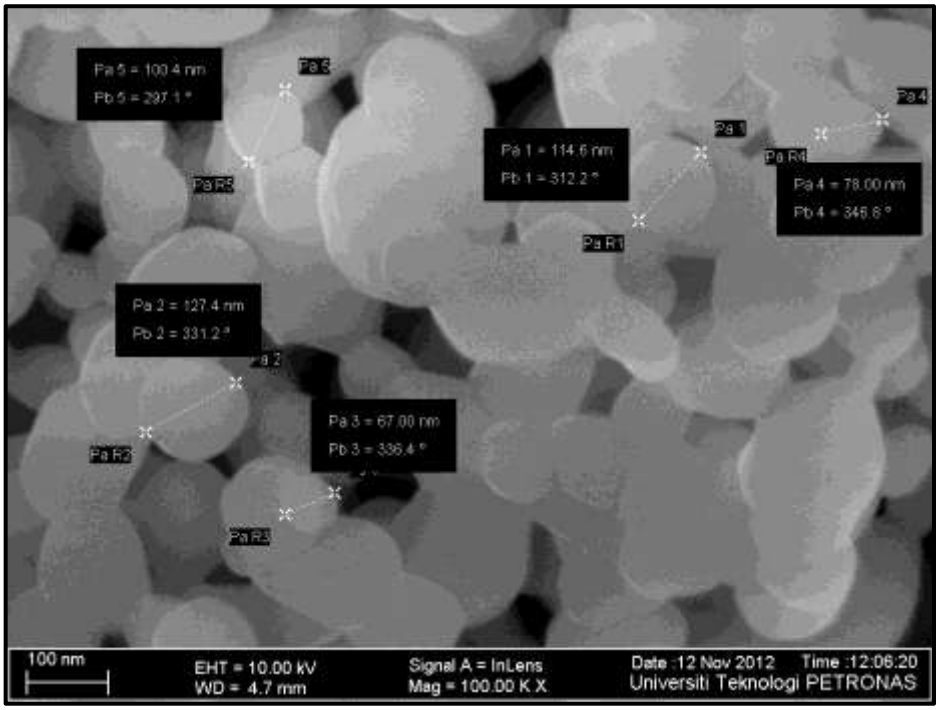

Figure 4.8: Diameters of the as-obtained S1 hematite nanocatalyst sample.

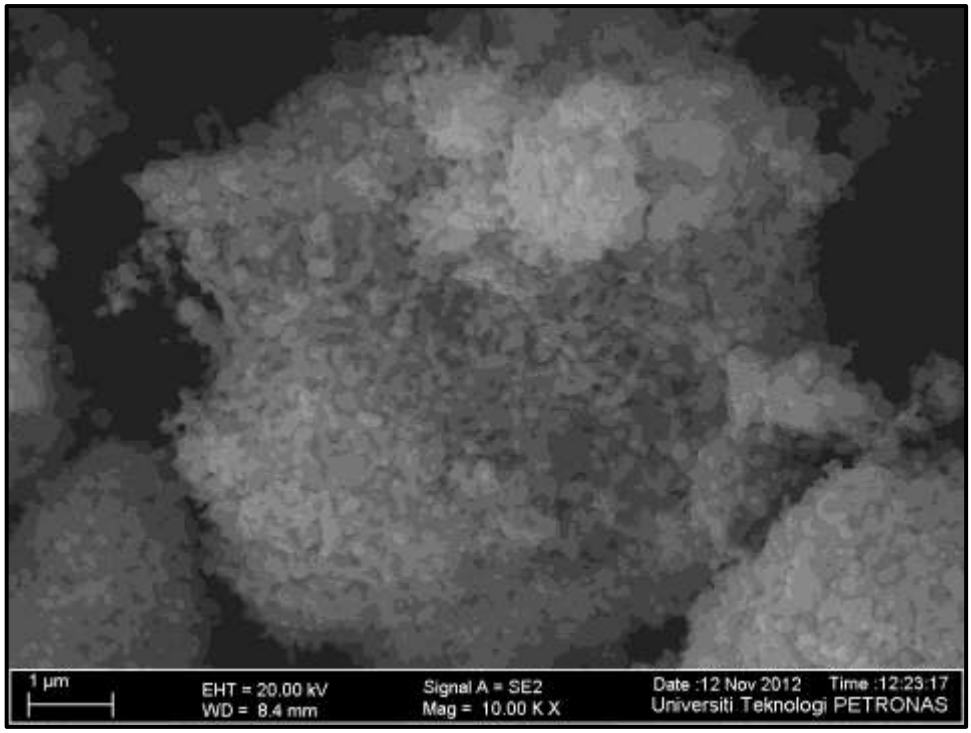

Figure 4.9: Distribution of S1 hematite nanocatalyst sample.

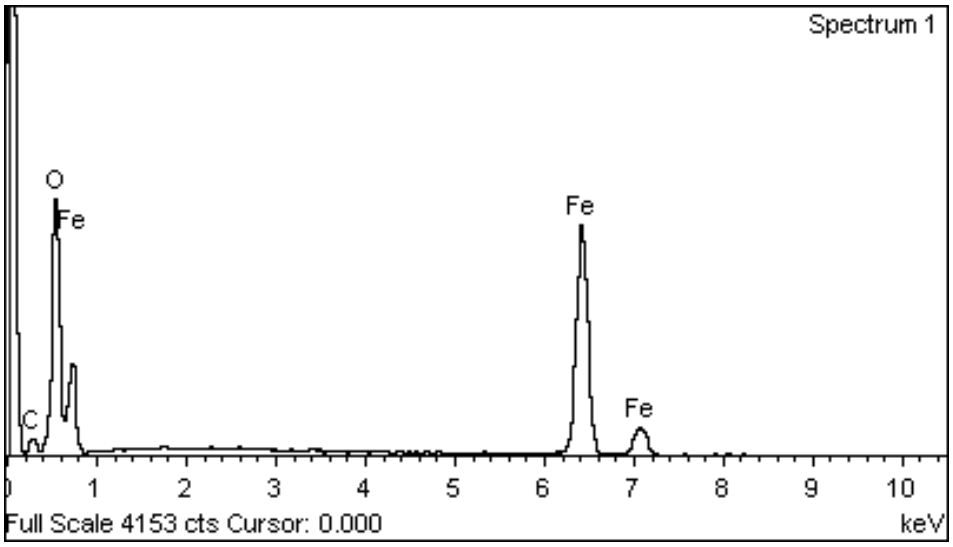

Figure 4.10: EDX spectrum of S1 hematite nanocatalyst sample.

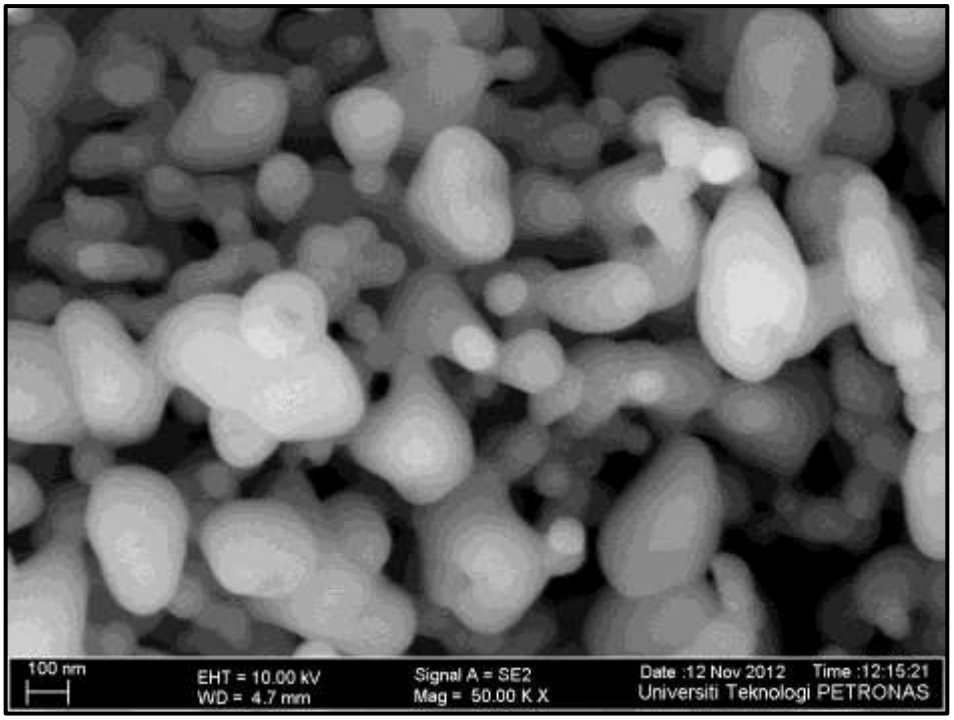

Figure 4.11: FESEM image of S4 hematite nanocatalyst sample.

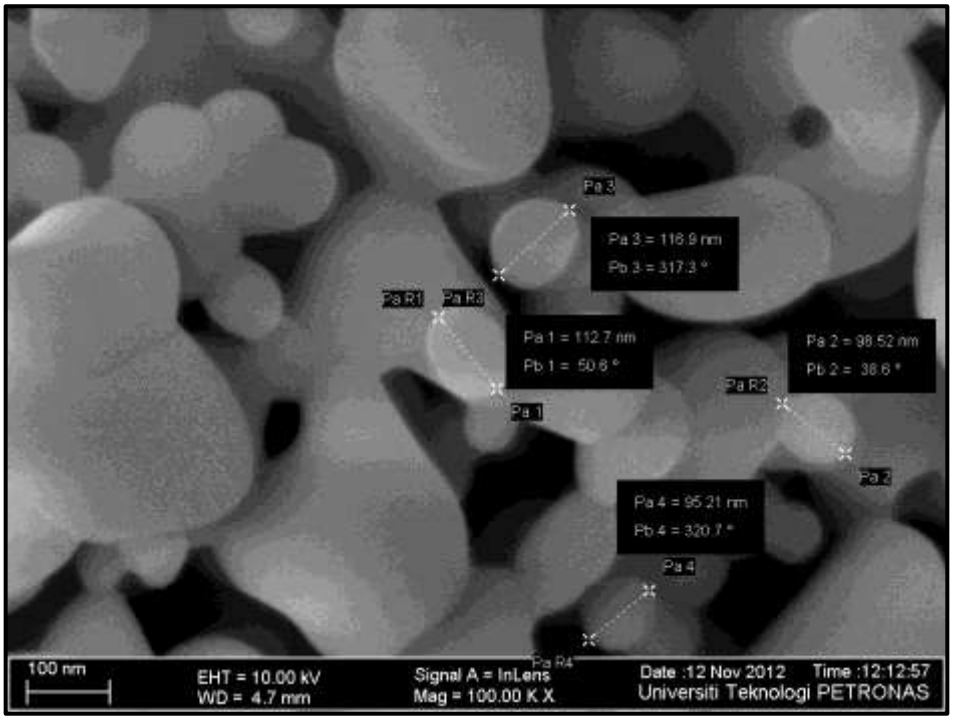

Figure 4.12: Diameters of the as-obtained S4 hematite nanocatalyst sample.

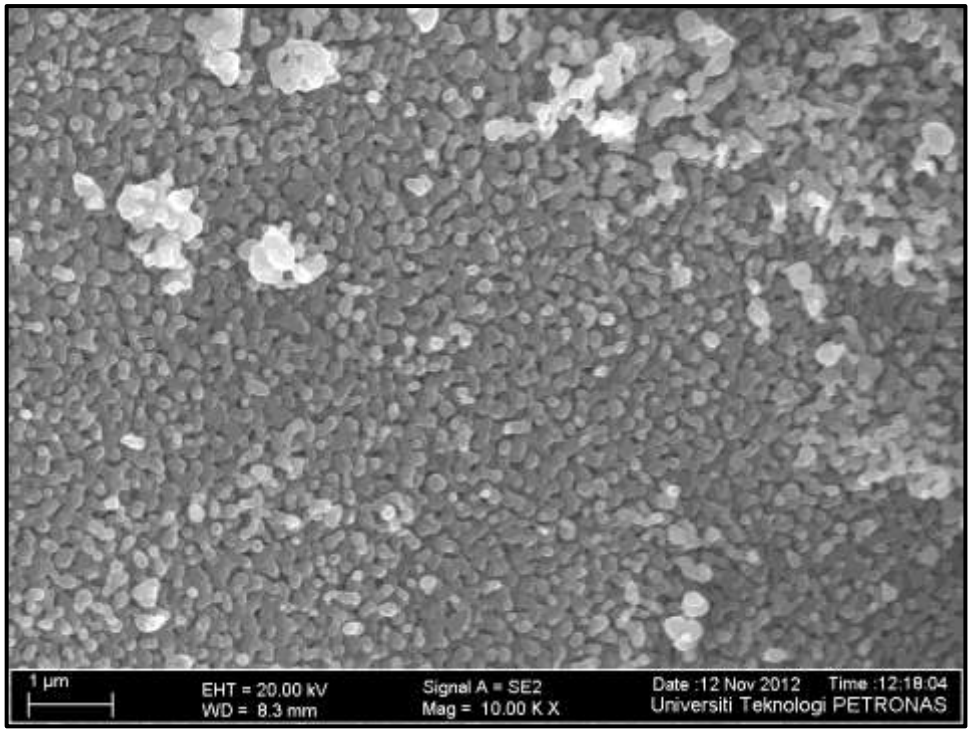

Figure 4.13: Distribution of S4 hematite nanocatalyst sample.

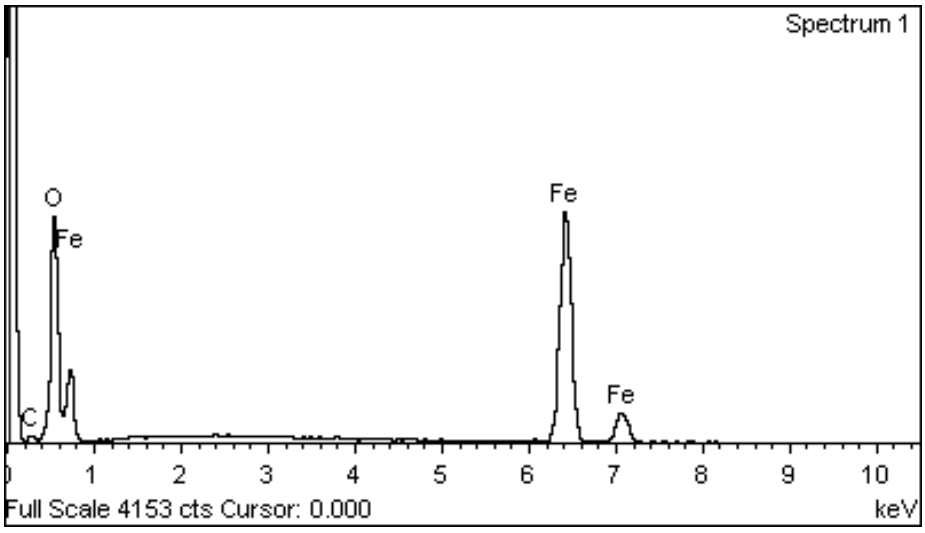

Figure 4.14: EDX spectrum of S4 hematite nanocatalyst sample.

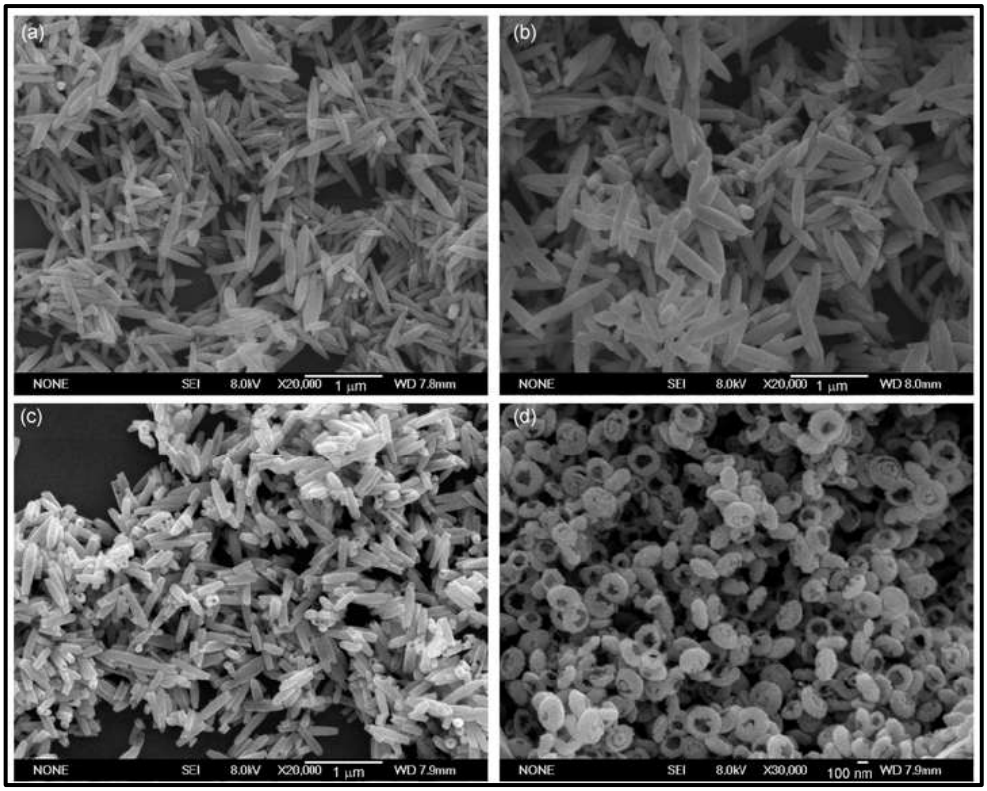

Figure 4.15: SEM images of hematite nanostructures synthesized by Liu et. al. [20]

4.2.4 Surface Area of Samples

The surface area of S1, S2, S3 and S4 hematite nanocatalyst samples were determined by using Brunauer-Emmett-Teller surface area analyser (BET) (Model: Micromeritics ASAP 2020 via nitrogen adsorption). The sample preparation was carried out in 2 stages, in which the first stage was carried out at 90^{o}C for 30 minutes at ramping rate of 10^{o}C/min. The second stage was carried out at 200^{o}C for 240 minutes at the same ramping rate of 10^{o}C/min. The BET surface area, pore volume and pore size of each of the hematite nanocatalyst sample are tabulated below.

Table 4.1: BET surface area of S1, S2, S3 and S4 hematite nanocatalyst samples.

Sample	BET surface area (m^2/g)
S1	5.4537
S2	5.9316
S3	6.0831
S4	7.6425

From the results obtained, it is shown that S4 hematite nanocatalyst sample has the highest surface area, which is 7.6425 m^2/g. This is followed by sample S3 with surface area of 6.0831 m^2/g and sample S2 with surface area of 5.9316 m^2/g. Sample S1 has the lowest surface area, which is 5.4537 m^2/g. From here, it is obvious that the BET surface area increases as the stirring period increases. This can be explained from the experiment. As the stirring period is increased, the mixture of iron (III) nitrate and nitric acid will have more time to react with each other and the particles can disperse themselves evenly throughout the solution. This will prevent the particles from agglomerate together and thus giving higher surface area.

Based on the research works done by Juncosa (2008), it is found that the BET surface area of hematite is 14.92 m^2/g [23]. Besides that, Wu et. al. (2006) stated that the BET surface areas of the hematite nanostructures synthesized using improved synthetic strategy range from 5.9 to 52.3 m^2/g [13]. From here, it can be seen that the BET surface areas of the four hematite nanocatalyst samples are slightly lower than that from the studies. This might be due to the agglomeration of the particles which caused the nitrogen hard to be adsorbed into the particles during the BET analysis, thus leading to lower surface area of the samples.

4.3 Measurement of Photocatalytic Activity

For the measurement of photocatalytic activity, all four samples are being tested in order to determine which sample can produce more hydrogen gas from water. From the experiment, it is found that S4 sample produced highest amount of hydrogen gas among the four samples. For 1g of S4 hematite nanocatalyst in 100 mL of distilled water, 4.75×10^{-3} mg/s of hydrogen gas is being produced during 15 minutes of the experiment. This is followed by S3 sample with 4.35×10^{-3} mg/s of hydrogen gas produced and S2 sample which produced 4.09×10^{-3} mg/s of hydrogen gas for the same period of time. S1 sample produced the least amount of hydrogen gas which had the value of 6.59×10^{-4} mg/s of hydrogen. The summary of the amount of hydrogen gas produced is shown in the table below.

Table 4.2: Amount of hydrogen gas produced from S1, S2, S3 and S4 hematite nanocatalyst samples.

Sample	Amount of hydrogen produced (mg/s)
S1	6.59E-04
S2	4.09E-03
S3	4.35E-03
S4	4.75E-03

The amount of hydrogen gas produced from the hematite nancatalyst samples can be explained from the BET surface areas of the samples. The higher the BET surface area of the samples, the higher the amount of hydrogen gas produced from the samples. This is because the higher surface area of hematite results in more active sites on the particles. With more active sites available, the reactions to produce hydrogen gas from the water molecules using the equations as shown below can take place effectively.

Oxidation: $H_2O + 2\ h^+ \rightarrow 2\ H^+ + (1/2)\ O_2$ **(11)**

Reduction: $2\ H^+ + 2\ e^- \rightarrow H_2$ **(12)**

Overall reaction: $H_2O \rightarrow H_2 + (1/2)\ O_2$ **(13)**

CHAPTER 5

CONCLUSION AND RECOMMENDATIONS

5.1 Conclusion

In summary, the hematite nanocatalyst samples synthesized using self-combustion method are proven to be rhombohedral crystalline hematite (α-Fe_2O_3) from XRD results. The hematite nanocatalyst showed spherical in shape as depicted in the FESEM images obtained. The diameters of the hematite samples were ranging from 60-140 nm which showed that they were in nano size. The BET surface area of the four samples increased with increasing stirring period. This affects the photocatalytic performance of the hematite samples in producing hydrogen gas from water. The amount of hydrogen gas produced increased with increasing surface area of the samples due to more active sites available on the particles.

5.2 Recommendations

As an improvement to the project, the project could be continued in the future by altering the parameters during the synthesis of hematite nanocatalyst in order to observe the effects on their morphologies and microstructures. Besides that, different synthesis method could be used to synthesize hematite nanocatalyst to obtain different hematite nanostructures. Apart from that, the photocatalytic water splitting by using hematite could be improved further to obtain more hydrogen gas. Overall, further studies on the hematite nanocatalyst and its performance in photocatalytic water splitting are suggested.

REFERENCES

1. Kudo, A. (2006). Development of photocatalyst materials for water splitting. *International Journal of Hydrogen Energy 31*, 197-202.

2. Kudo, A. (2007). Photocatalysis and solar hydrogen production. *Pure Appl. Chem.*, 1917-1927.

3. Kudo, A., & Miseki, Y. (2009). Heterogeneous photocatalyst materials for water splitting. *Chemical Society Review*, 253-278.

4. Fujishima, A., Rao, T. N., & Tryk, D. A. (2000). Titanium dioxide photocatalysis. *Journal of Photochemistry and Photobiology*, 1-21.

5. Lian, X., Yang, X., Liu, S., Xu, Y., Jiang, C., Chen, J., et al. (2010). Enhanced photoelectrochemical performance of Ti-doped hematite thin films prepared by the sol–gel method. *Applied Surface Science 258*, 2307-2311.

6. Wang, R., Chen, Y., Fu, Y., Zhang, H., & Kisielowski, C. (2005). Bicrystalline Hematite Nanowires. *J. Phys. Chem. B*, 12245-12249.

7. Hiralal, P., Saremi-Yarahmadi, S., Bayer, B. C., Wang, H., Hofmann, S., Wijayantha, K. U., et al. (2011). Nanostructured hematite photoelectrochemical electrodes prepared by the low temperature thermal oxidation of iron. *Solar Energy Materials & Solar Cells*, 1819-1825.

8. Souza, F. L., Lopes, K. P., Nascente, P. A., & Leite, E. R. (2009). Nanostructured hematite thin films produced by spin-coating deposition solution: Application in water splitting. *Solar Energy Materials & Solar Cells 93*, 362-368.

9. Chiarello, G. L., Forni, L., Rossetti, I., & Selli, E. (n.d.). Photocatalytic water splitting on different oxide-based systems.

10. Sreethawong, T., Junbua, C., & Chavadej, S. (2009). Photocatalytic H_2 production from water splitting under visible light irradiation using Eosin Y-sensitized mesoporous-assembled Pt/TiO_2 nanocrystal. *Journal of Power Sources 190*, 513-524.

11. Townsend, T. K., Sabio, E. M., Browning, N. D., & Osterloh, F. E. (2011). Photocatalytic water oxidation with suspended alpha-Fe_2O_3 particles-effects of nanoscaling. *Energy & Environmental Science*, 4270-4275.

12. Yerga, R. M., Galvan, M. C., Valle, F. d., Mano, J. A., & Fierro, J. L. (2009). Water Splitting on Semiconductor Catalysts under Visible-Light Irradiation. *ChemSusChem*, 471-485.

13. Wu, C., Yin, P., OuYang, C., & Xie, Y. (2006). Synthesis of Hematite (α-Fe_2O_3) Nanorods: Diameter-Size and Shape Effects on Their. *J. Phys. Chem. B*, 17806-17812.

14. Liu, L., Kou, H.-Z., Mo, W., Liu, H., & Wang, Y. (2006). Surfactant-Assisted Synthesis of α-Fe_2O_3 Nanotubes and Nanorods with Shape-Dependent. *J. Phys. Chem. B*, 15218-15223.

15. Zeng, S., Tang, K., & Li, T. (2007). Controlled synthesis of α-Fe_2O_3 nanorods and its size-dependent optical. *Journal of Colloid and Interface Science*, 513-521.

16. Vincent, T., Gross, M., Dotan, H., & Rothschild, A. (2012). Thermally oxidized iron oxide nanoarchitectures for hydrogen production by solar-induced water splitting. *International Journal of Hydrogen Energy*, 8102-8109.

17. Kim, J. G., Han, K. H., Lee, C. H., & Jeong, J. Y. (2001). Crystallographic and Magnetic Properties of Nanostructured Hematite Synthesized by the Sol-Gel Process. *Journal of the Korean Physical Society*, 798-802.

18. Latunde, O. (2008). Synthesis of Nanostructured Iron Oxide Thin Films for Photocatalytic Hydrogen Production. *NNIN REU Research Accomplishments*, 44-45.

19. Saremi-Yarahmadi, S., Vaidhyanathan, B., & Wijayantha, K. U. (2010). Microwave-assisted low temperature fabrication of nanostructured α-Fe_2O_3 electrodes for solar-driven hydrogen generation. *International Journal of Hydrogen Energy 35*, 10155-10165.

20. Liu, C., Ma, J., & Liu, Y. (2011). Formation mechanism and magnetic properties of three different hematite nanostructures synthesized by one-step hydrothermal procedure. *SCIENCE CHINA*, 1607-1614.

21. Akbar, S., Hasanain, S. K., Azmat, N., & Nadeem, M. (n.d.). Synthesis of Fe_2O_3 nanoparticles by new Sol-Gel method and their structural and magnetic characterizations.

22. Han, Q., Xu, Y. Y., Fu, Y. Y., Zhang, H., Wang, R. M., Wang, T. M., et al. (2006). Defects and growing mechanisms of α-Fe_2O_3 nanowires. *Chemical Physics Letters*, 100-103.

23. Juncosa, E. C. (2008). Adsorption Properties of Synthetic Iron Oxides: As (V) Adsoprtion on Geothite (α-FeOOH). *D Master Thesis*, 2-31.

24. Jiang, X., & Yu, A. (2009). *Journal of Materials Processing Technology 209*, 4558-4562.